Kaleidoscopic Spatial Instability: Bifurcations of Optical Transverse Solitary Waves

J. W. Grantham, H. M. Gibbs, G. Khitrova, J. F. Valley,[a] and Xu Jiajin
Optical Sciences Center, University of Arizona, Tucson, Arizona 85721
(Received 12 September 1990)

The cell-exit transverse profile for one-way propagation through sodium vapor forms a pattern of spots with complexity and beauty rivaling that of a kaleidoscope. These patterns are stationary in time, reproduce completely when the power or frequency is scanned, and agree well with one-way computations that show that the patterns change very little after one-fifth of the propagation distance, i.e., they exhibit the properties of bifurcations of transverse solitary waves.

PACS numbers: 42.50.Tj, 42.50.Qg, 42.65.Jx

Recently there has been increased emphasis on spatial instabilities, but mainly theoretical and mainly with cavities or counterpropagating beams.[1,2] Here we present a spatial instability, with transverse feedback but free from longitudinal feedback, in which a beam propagating in one direction in a self-focusing medium breaks up into a pattern of filaments that bifurcates nonlinearly as the input power is increased. This experimental arrangement reduces spatial instabilities to the bare essentials, permitting us to make the first comparison between experimental solitary-wave bifurcations and theoretical calculations. Optical transverse solitary waves have appeared numerically in a bistable self-focusing ring cavity and in one-way propagation in linear waveguides with self-focusing claddings.[3] In those cases and here, *the physics of the formation of the solitary waves is the competition between self-focusing and diffraction leading to the eigenmodes of propagation, i.e., to the solitary-wave solutions of nonlinear Schrödinger-type equations.*

Our cell-exit spatial patterns are stable, even though they may jitter a little, and *are highly reproducible as the input power is scanned up and down, showing that they are seeded by fixed-phase variations across the input profile and not by random fluctuations.*[4] The inherent fixed-phase variations on our experimental input profile were made very small by spatial filtering; then we intentionally introduced much larger aberrations that enhanced the complexity of the patterns (as many as eleven spots). Excellent agreement is shown below between numerical simulations and experimental data for pattern bifurcations as a function of intensity or detuning with a simple input aberration or shift of the input beam waist. The input aberration or curvature introduces some wave-vector selectivity, just as cavity modes introduce frequency selectivity for temporal instabilities.

The instability nature of this phenomena is emphasized by the slowness (on the order of 1 s) with which the reproducible pattern is regained after the beam is momentarily interrupted by inserting a card by hand. Removal of the card turns on the light slowly ($\cong$ milliseconds) and asymmetrically. This results in the filamentation locking onto the "wrong" pattern (local basin of attraction); often a very long time is required before a large fluctuation allows the system to escape the local minimum and reach the steady-state pattern (global minimum) from which it never escapes.

The $\cong$800-mW single-mode output power of a dye laser is collimated and brought to a waist at the cell entrance, with a maximum of 500 mW reaching the $\simeq$265 °C 10-cm-long evacuated quartz cell containing sodium at a density of 5.7×10^{13} cm^{-3}. The laser beam is vertically linearly polarized and always travels horizontally. The transverse spatial profile of the laser beam as it leaves the sodium (cell-exit profile) is magnified and imaged onto a charge-coupled-device camera, recorded on video tape, and then digitized into a 256×256 array of intensity values. A Fabry-Pérot interferometer (flat mirrors with $R=0.98$, finesse of 100, and 7.5-GHz free spectral range) was used to study the frequency spectrum of the output beam after recollimation. The detuning $\delta\nu$ of the laser frequency to the high-frequency side of the D_2 resonance of sodium is measured with Lamb-dip spectroscopy, with zero defined as the midpoint between the two hyperfine transitions. Since any type of inhomogeneity or aberration in the input beam can cause beam filamentation,[5] great care was taken to spatially filter the beam, to carefully clean and align the input optics, and to choose a spot on the cell window with minimal aberration.

The first intentionally introduced aberration was *astigmatism induced by using two cylindrical lenses* of focal length 21 cm. The y waist was at the input window, while the position of the x waist was varied inside the sodium cell; see Fig. 1. Figure 2 shows a solitary-wave bifurcation route, with the x waist 3 cm inside the sodium cell (in the absence of sodium), in excellent agreement with our computations, described below.

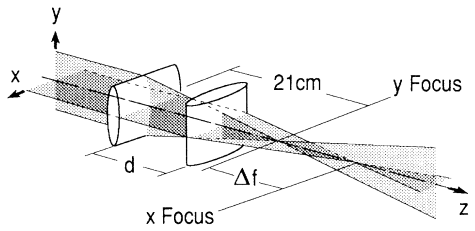

FIG. 1. Arrangement of cylindrical lenses to introduce controllable astigmatism; the origin of z is the input window, i.e., the beginning of the sodium vapor. For Fig. 2, $d=\Delta f=3$ cm; for Fig. 3, $d=\Delta f=8$ cm.

These computations show that the beam focuses to a new waist of $\cong$ 15 μm before expanding and forming three independent beams by $z \cong 3$ cm. The beam separation increases linearly by a factor of 3 between $z=3$ and 10 cm, but the solitary-wave *pattern* does not change.

The propagation and pattern formation of the input laser beam E_1 is computed in the paraxial and slowly-varying-envelope approximations:

$$\nabla_T^2 A_1 + 2ik_1 \partial A_1/\partial z = -\alpha_1 A_1 , \quad (1)$$

where

$$E_1(x,y,z,\omega_1) = A_1(x,y,z,\omega_1)\exp[i(k_1 z - \omega_1 t)] ,$$

$$k_1 = 2\pi\omega_1/c, \quad \nabla_T^2 = \partial^2/\partial x^2 + \partial^2/\partial y^2 .$$

The coefficient $\alpha_1(x,y,z)$ is a function[6] of A_1 and ω_1 has been integrated over the Doppler velocity distribution; it includes both nonlinear absorption (gain) and refraction, leading to the pattern formation. Equation (1) is solved in 3 CPU minutes on a CRAY computer using fast-Fourier-transform techniques.[7-9] To model the intentionally introduced astigmatism, a phase term was added to the input wave front at the cell entrance such that the slowly varying input field envelope has the following form:

$$A_1(x,y,0,\omega_1) = A_1'(0,\omega_1)\exp\left[\frac{-ik_1}{2}\left(\frac{x^2}{q_x}+\frac{y^2}{q_y}\right)\right], \quad (2)$$

where $q_x = -\Delta f_x + i\pi w_0^2/\lambda$, $q_y = -\Delta f_y + i\pi w_0^2/\lambda$, λ is the input wavelength, and Δf_x (Δf_y) is the distance between the x (y) focal point and the cell entrance window. Here, with $\Delta f_x = 3.0$ cm and $\Delta f_y = 0$, the phase difference between $x=0$ and $x=w_0=52$ μm is $\cong\lambda/13$.

This astigmatic bifurcation sequence is more complicated as one gets closer to resonance and increases the astigmatism (increases the separation between the two orthogonal foci) for a given sodium density. In this case, the bifurcation sequence can be one spot $\rightarrow$ three spots $\rightarrow$ two spots $\rightarrow$ three spots and more complicated. Generally, as the laser pump power is increased, the number of spots and their spatial separation increases, but both the computer simulations and the experiment show that spatial and number contraction can occur, most likely arising from the oscillations in beam diameter accompanying quasitrapping of the pump beam.[8]

Figure 3 shows the bifurcation sequence as the laser pump detuning is increased from -0.7 to 7 GHz. The no-sodium x waist is 8 cm inside the sodium cell ($\Delta f_x = 8.0$ cm) and the laser power is 200 mW. When the detuning is larger than 4 GHz, the bifurcation process begins what we call the kaleidoscope sequence where the patterns become quite complicated with little apparent symmetry, perhaps approaching spatial chaos.[10] The computational patterns show good qualitative agreement with the experimental patterns.[11]

The other perturbation was an *input-beam convergence* (phase $\sim r^2$), introduced experimentally by changing the collimation of the light reaching the 30-cm focusing lens and computationally by a focus phase term. Figures 4(a')-4(d') show the experimental bifurcation sequence. Comparing our experimental spatial patterns with known optical spot diagrams,[12] we concluded that the primary residual aberrations responsible for the slightly noncircular symmetry of the data are astigma-

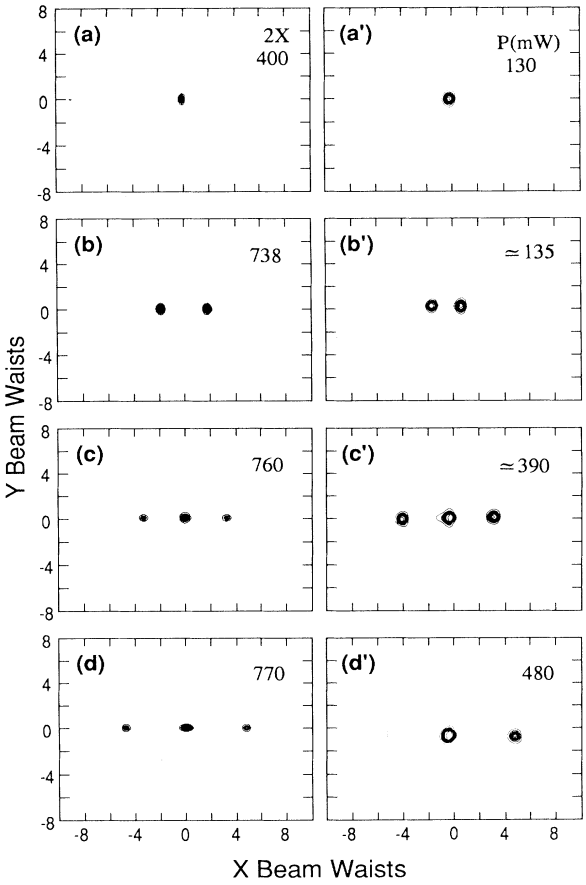

FIG. 2. Cell-exit profiles for a power bifurcation sequence with astigmatism applied to the input laser beam. Computational patterns (a)-(d): on-resonance absorption $\alpha_0 = 24000$ cm^{-1} [before Doppler broadening (Ref. 14)]; frequencies, in units of $1/2\pi t_1 = 10$ MHz, are pump detuning of $\Delta = +430$ from the low-power atomic resonance and Rabi frequency (maximum value at the entrance of the cell) $2X$ equal to (a) 400, (b) 738, (c) 760, and (d) 770. $T_2 = 2T_1$; single resonance with Doppler broadening of $ku = 105$. Corresponding experimental patterns (a')-(d'): pump detuning $\delta\nu = +3.4$ GHz; unsaturated transmission $T = 0.36$ at +3.4 GHz; input laser power P (mW) of (a') 130, (b') $\cong$135, (c') $\cong$390, and (d') 480; $^2S_{1/2}$-$^2P_{3/2}$ D_2 transition with 1.8-GHz ground-state hyperfine transition. The contour lines range from 34 to 158 W/cm^2 in 11.3-W/cm^2 increments. At low powers, no beam exits the cell because of the high absorption. The threshold power for seeing a single filament is about 45 mW; generally, Raman gain accompanies filament formation.

tism and coma, modeled by two asymmetric phase terms:

$$A_1(x,y,0,\omega_1)=A_1'(0,\omega_1)\exp\left\{-\left[\left(\frac{1}{w^2}+\frac{i\pi}{\lambda R}\right)r^2+2\pi\left(\frac{W_{22}y^2}{w^2}+\frac{W_{13}r^2y}{w^3}\right)\right]\right\}, \quad (3)$$

where w is the beam radius at the cell entrance, λ is the input field wavelength, R is the radius of curvature at the cell entrance, W_{22} is the astigmatic coefficient, W_{13} is the comatic coefficient, and $r^2=x^2+y^2$. $W_{22}=5\times10^{-4}$ and $W_{13}=5\times10^{-5}$ were used in Figs. 4(a)–4(d) to match the data of Figs. 4(a′)–4(d′). The phase difference between $r=0$ and $r=w$ is $\cong\lambda/7$ for the focus term, while it is only $\lambda/2000$ for astigmatism and $\lambda/20000$ for coma (making it almost impossible to measure them directly). The computations show that in Fig. 4(d) the input focuses to a waist of $0.14w_0$ at $z=0.67$ cm before expanding to form a six-beam solitary wave by $z=2$ cm.

This spatial instability is accompanied by the generation of one or more new frequencies, resulting in temporal instabilities as well. The new frequencies (measured using a Fabry-Pérot interferometer) arise from the Raman-gain portion of the intense-field, Doppler-broadened sodium absorption-gain profile.[13–16] This inseparability of spatial and temporal instabilities comes from the fact that the power required for filament formation is about the same as the threshold for Raman gain.

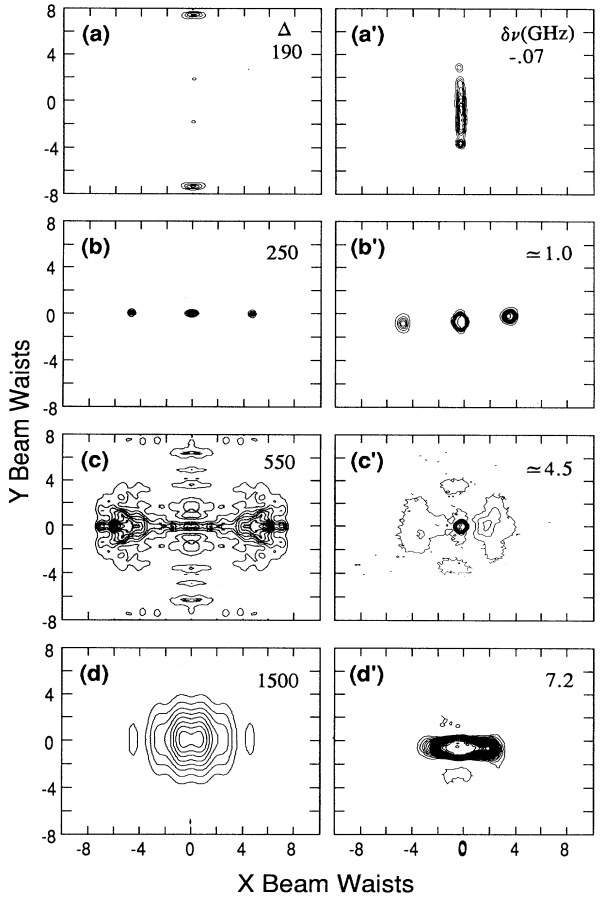

FIG. 3. Cell-exit profiles for a pump-detuning bifurcation sequence with astigmatism applied to the input laser beam. Computational patterns (a)–(d): $\alpha_0=24000$ cm^{-1}; $2X=540$; Δ ranges from (a) +190 to (d) +1500; $T_2=2T_1$; $ku=105$. Corresponding experimental patterns (a′)–(d′): $P=200$ mW; $\delta\nu$ ranges from (a′) −0.7 to (d′) 7.2 GHz; $T=0.36$ at +3.4 GHz. The contour lines in (a′), (c′), and (d′) range from 13.6 to 133 in intervals of 5.67 W/cm^2; in (b′), they range from 34 to 147 in 11.3-W/cm^2 increments.

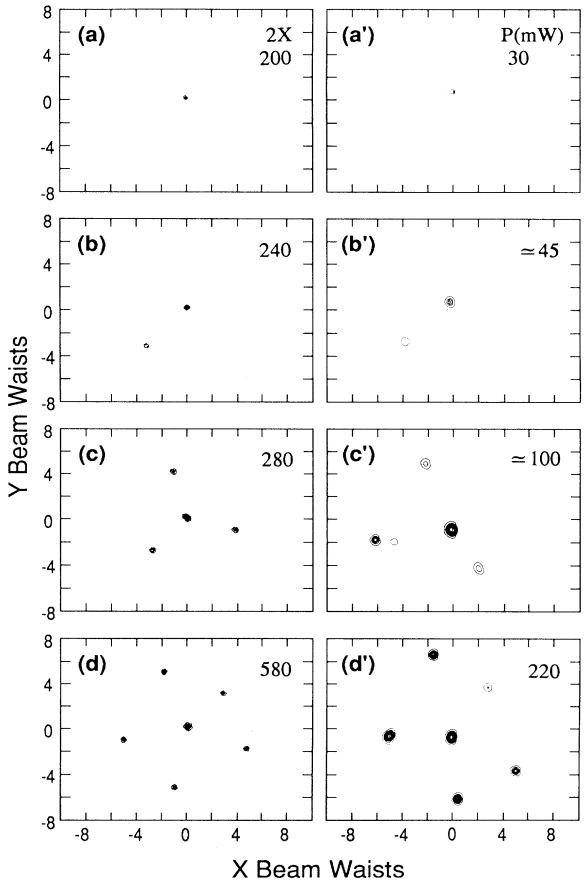

FIG. 4. Cell-exit profiles for a power bifurcation sequence with focus added to the input laser beam. Computational patterns (a)–(d): $\alpha_0=24000$ cm^{-1}; $\Delta=+290$; $2X$ equal to (a) 200, (b) 240, (c) 280, and (d) 580; $T_2=2T_1$; $ku=105$. Corresponding experimental patterns (a′)–(d′): $\delta\nu=2$ GHz; P ranges from (a′) 30 mW to (d′) 200 mW; $T=0.0$ at +2.0 GHz and 0.36 at +3.4 GHz; the contours are the same as in Fig. 2 except for a maximum of 147 W/cm^2. $R=-3.5$ cm and $w=76.3$ μm (at $z=0$) for both the experimental and computational patterns.

The spectrum of each filament contains the input pump frequency and new Raman-gain frequencies, but the spatial pattern is determined by light at the pump frequency alone if the new frequencies contain little power. Such was the case for all of the data used here for comparisons with our single-frequency computations. The spectrum of a single filament sometimes consists of two regions; from their dependence upon the intensity and detuning, we believe this is the first observation of the double-peaked Raman gain predicted by Khitrova and coworkers.[14,16]

In conclusion, we have observed spatial bifurcation sequences as interesting and complicated as temporal bifurcation sequences observed in other optical systems. They are explained as spatial instabilities seeded by intentionally introduced aberrations. In temporal instabilities, the ω gain curve determines which frequencies in the fluctuations will be amplified; selective feedback or an injected signal is used to encourage particular directions or frequencies. In spatial instabilities, the k gain curve determines which wave vectors in the fluctuations will be amplified; input-wavefront-phase encoding is used to accentuate particular wave vectors, resulting in complicated bifurcations as a function of intensity or detuning. In self-induced transparency,[17] the solitons of pulse propagation have areas of 2π, 4π, ... in order that no energy be left in the highly absorbing medium. The solitary waves here permit a cw beam to propagate through a highly absorbing medium by forming transparent waveguides in which the absorption is bleached in the center of each filament. The input-phase encoding breaks the symmetry, stabilizes the spatial pattern, and makes it possible to study spatial-pattern bifurcations free of time dynamics.[18]

The authors are grateful for support from the U.S. Air Force Office of Scientific Research and the Army Research Office, for use of the CRAY computer at Kirtland Air Force Base, and for helpful discussion with E. Wright and G. Benza.

---

[a]Present address: Lockheed Palo Alto Research Laboratories, 3251 Hanover Street, Palo Alto, CA 94304-1187.

[1]Special issue on *Transverse Effects in Nonlinear-Optical Systems,* edited by N. Abraham and W. Firth [J. Opt. Soc. Am. B **7**, 948–1157 (1990); **7**, 1264–1373 (1990)].

[2]*Proceedings of the Conference on Nonlinear Dynamics in Optical Systems, Afton, Oklahoma, 1990* (Optical Society of America, Washington, DC, 1990).

[3]J. V. Moloney and H. M. Gibbs, Phys. Rev. Lett. **48**, 1607 (1982); D. W. McLaughlin, J. V. Moloney, and A. C. Newell, Phys. Rev. Lett. **51**, 75 (1983); **54**, 681 (1985); J. V. Moloney, Phys. Rev. Lett. **53**, 556 (1984); Phys. Rev. A **33**, 4061 (1986). For computations of propagationally unstable 3D solitary waves in a nonlinear slab waveguide, see D. R. Heatley, E. M. Wright, and G. I. Stegeman, Appl. Phys. Lett. **56**, 215 (1990), and in a fiber with a linear core and self-focusing cladding, see D. R. Heatley, E. M. Wright, and G. I. Stegeman, Opt. Lett. (to be published).

[4]This spatial instability is different from the *far-field* spots of G. Grynberg, Opt. Commun. **66**, 321 (1988), that require a standing wave, and from the far-field patterns of G. Guisfredi, J. F. Valley, R. Pon, G. Khitrova, and H. M. Gibbs, J. Opt. Soc. Am. B **5**, 1181 (1988), that arise from modes of a resonator consisting of a four-wave-mixing mirror and an ordinary mirror (see also M. LeBerre, E. Ressayre, and A. Tallet, in Ref. 1, p. 1346).

[5]A. J. Campillo, S. L. Shapiro, and B. R. Suydam, Appl. Phys. Lett. **23**, 628 (1973).

[6]M. D. Levenson, *Introduction to Nonlinear Laser Spectroscopy* (Academic, New York, 1982), Sec. 2.6. Our expressions in terms of plasma dispersion functions are given in J. F. Valley, Ph.D. dissertation, Optical Sciences Center, University of Arizona, 1989 (unpublished).

[7]J. V. Moloney, M. R. Belic, and H. M. Gibbs, Opt. Commun. **41**, 379 (1982), and references therein.

[8]M. LeBerre, E. Ressayre, A. Tallet, and F. P. Matter, J. Opt. Soc. Am. B **2**, 956 (1985), and references therein.

[9]J. F. Valley, G. Khitrova, H. M. Gibbs, J. W. Grantham, and Xu Jiajin, Phys. Rev. Lett. **64**, 2362 (1990).

[10]W. J. Firth, Phys. Rev. Lett. **61**, 329 (1988).

[11]Various approximations prevent exact quantitative correspondence between the experimental and computational detunings. Sodium is treated as a single Doppler-broadened, two-level transition, with a detuning usually corresponding to complete hyperfine optical pumping. We measure the unsaturated transmission at +3.4 GHz and from this value calculate the absorption value used in the computations. One should not be concerned with the opposite signs of Δ and $\delta\nu$ in Figs. 3(a) and 3(a'). A $\delta\nu=-0.7$ GHz is still 0.2 GHz on the focusing side of the most-strongly-absorbing hyperfine component. It is clear experimentally that the nonlinear self-action is still self-focusing; for example, in Fig. 3(a') the x waist is reduced going through the cell.

[12]Optical spot diagrams are a common output of commercial lens-design programs.

[13]S. Haroche and F. Hartmann, Phys. Rev. A **6**, 1280 (1972).

[14]G. Khitrova, Ph.D. dissertation, Department of Physics, New York University, 1986 (unpublished).

[15]G. Khitrova, J. F. Valley, and H. M. Gibbs, Phys. Rev. Lett. **60**, 1126 (1988).

[16]G. Khitrova, P. R. Berman, and M. Sargent, III, J. Opt. Soc. Am. **5**, 160 (1988).

[17]S. L. McCall and E. L. Hahn, Phys. Rev. Lett. **18**, 908 (1967); H. M. Gibbs and R. E. Slusher, Phys. Rev. Lett. **24**, 638 (1970).

[18]We have seen time-independent spatial patterns in ring cavities as well; probably there, too, the apparatus breaks the cylindrical symmetry and stabilizes the temporal instabilities found using maps and attributed to spontaneous spatial symmetry breaking by A. Ouarzeddini, H. Adachihara, J. V. Moloney, D. W. McLaughlin, and A. C. Newell, J. Phys. (Paris), Colloq. **49**, C2-455 (1988).